Brownian dynamics simulation of orientational behavior, flow-induced structure, and rheological properties of a suspension of oblate spheroid particles under simple shear

Takehiro Yamamoto,* Takanori Suga, and Noriyasu Mori†
Department of Mechanophysics Engineering, Osaka University, 2-1, Yamadaoka, Suita, Osaka 565-0871, Japan
(Received 20 December 2004; revised manuscript received 20 June 2005; published 24 August 2005)

Brownian dynamics (BD) simulations were carried out for suspensions of oblate spheroid particles interacting via the Gay-Berne (GB) potential. The oblate spheroid particles were applied as a model of disc-like particles and the system of suspension of the particles was considered. Numerically analyzed were both the change in phase with the number density of the particles at equilibrium state and the behavior of the particles in simple shear flows. The system changed from isotropic phase to nematic one with increasing the particle concentration. In the simulation of shear flows, the shear was imposed upon the systems in nematic phase at equilibrium. The systems exhibited various motions of the director depending on the shear rate, e.g. the continuous rotation of director at low shear rates, the wagging at moderate shear rates, and the flow aligning at high shear rates. Temporal change in inner structure of suspensions was also analyzed and collapse of initial particle configurations due to shear was found. Moreover, rheological properties of the suspension were investigated. The numerical simulation predicted the shear-thinning in viscosity, negative first normal stress difference, and positive second normal stress difference, and these results qualitatively agreed with the predictions using a constitutive equation for discotic nematics. The present study proved that the BD simulation using spheroid particles interacting via the GB potential is an effective approach for investigating the flow behavior and flow-induced structure of suspensions of disklike particles at a particulate level.

DOI: 10.1103/PhysRevE.72.021509 PACS number(s): 83.10.Mj, 82.70.−y, 82.70.Kj, 47.17.+e

I. INTRODUCTION

Flow-induced structures of suspensions and the relation between the structural change and the particle motion in suspensions are interesting subjects in flow problems of suspensions. The Brownian dynamics (BD) simulation is a useful technique to investigate the structural change of suspensions at a particulate level. In the present study, we employed a suspension of oblate spheroid particles as a model of suspension of disklike particles and performed the BD simulation for the system under simple shear flows to analyze the orientational behavior of particles during the structural change. Furthermore, rheological properties of the suspension of oblate spheroid particles were evaluated using the results of the BD simulation.

Suspensions of disklike particles including clay, pitch, discotic liquid crystals are important materials in industry. For example, the kaolin is clay, including particles having platelike geometry and are widely applied to industrial materials such as paper, cosmetics, and ceramics. The rheological property of kaolin clay suspensions has been studied considering the flow-induced structure. Jogun and Zukoski [1] have investigated viscoelastic properties of dense kaolin clay suspensions. They discussed the relation between the rheology of kaolin suspensions and the microstructure in a shear flow based on a model for liquid crystalline polymer (LCP) suspensions. Recently, they have carried out x-ray scattering experiments to explore the flow properties and microstructure of kaolin suspensions and found that the fractional degree of orientation of the suspension was independent of volume fraction [2]. Brown *et al.* [3] have studied the orientational order in concentrated dispersions of kaolin particles under shear in a pipe and that in a plate-plate cell using a neutron diffraction technique. They investigated effects of the volume fraction and the shear rate on the particle alignment and the orientational order, and indicated that under shear disklike particles aligned with normals closer to the velocity gradient direction and the degree of order increased with shear rate. Moan *et al.* [4] have studied flow behavior of concentrated suspensions of kaolin particles in shear flows and rheological properties of the suspensions were investigated. They found that the flow curve showed a three-region shape similar to the curve obtained for LCPs and that the first normal stress difference took a negative steady-state value and the sign of the second normal stress difference depended on the shear rate. In experimental studies of suspensions of other disklike particles, Hammouda *et al.* [5] have performed small-angle neutron scattering (SANS) measurements to investigate shear-induced orientations of discotic liquid crystal micelles in aqueous solutions of the cesium-perfluorooctanoate under simple Couette and oscillatory shear. They found that the micelles oriented mostly parallel to the flow direction and observed a partial flipping of the orientation in the smectic phase. Brown and Rennie [6–8] have observed the shear-induced structure of the dispersion of monodispersed nickel hydroxide particles using neutron diffraction and SANS techniques [6,7] and polarized light microscopy [8]. In their studies, it was shown that the disks were aligned with normals in the flow at low shear rates and were aligned with their normals in the velocity gradient direction at high shear rates. In addition, phenomena implying a shear-induced phase separation were observed.

*Electronic address: take@mech.eng.osaka-u.ac.jp
†Electronic address: n.mori@mech.eng.osaka-u.ac.jp

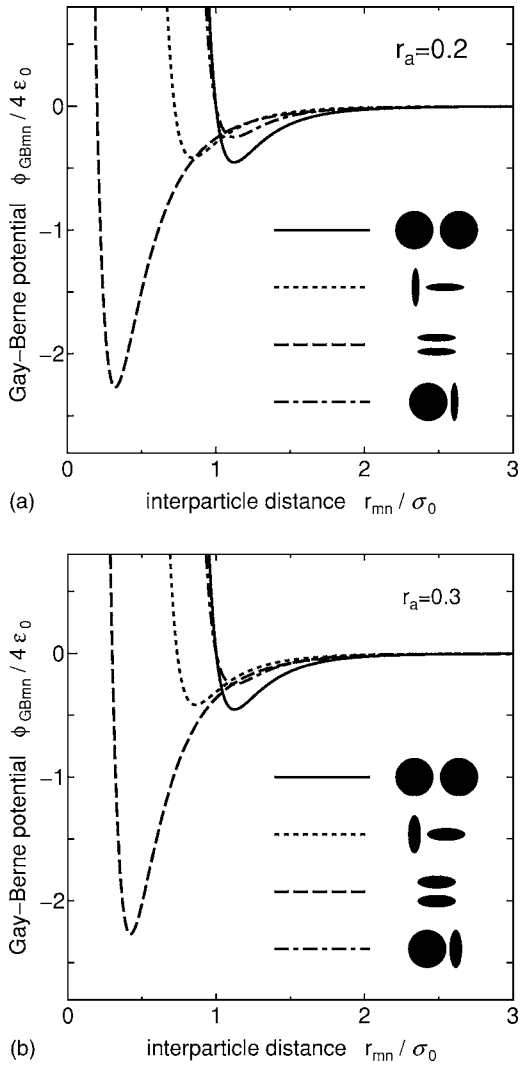

FIG. 1. Distance dependence of the Gay-Berne potential for the systems with r_a=0.2 (a) and 0.3 (b) for various configurations: ε_r =5 and (μ,ν)=(1,0.625) and (1, 1) for r_a=0.2 and 0.3, respectively. The circles and ellipsoids illustrate the configurations of particles. The rigid and dashed lines indicate results of the side-by-side and the end-to-end configurations, respectively.

In theoretical and numerical studies of the suspension of disklike particles, many studies have treated discotic nematics liquid crystals (DNLCs). Carlsson [9] has studied the signs of the Leslie viscosities α_2 and α_3 and predicted that α_3 should be positive for disklike molecules and the molecules show the flow aligning and the tumbling motion for positive α_2 and negative α_2, respectively. Carlsson [10] also numerically simulated the shear flow of nematic liquid crystals with $\alpha_3>0$ under an "in-plane" assumption to predict the director and velocity profiles and found the possibility of multivalued solutions for the tilt angle of the director. Singh and Rey [11,12] have developed constitutive equations for DNLCs and discussed the relation among rheological properties and the microstructure. The same authors [13] have analyzed the flow-induced structure of the discotic mesophase using a constitutive equation improved by incorporating long-range elasticity terms [14–16] and characterized the effects of long-range elasticity on the flow-induced microstructure. The effects of surface anchoring conditions and long-range elasticity on the flow-induced structure were investigated. Grecov and Rey [17] have numerically analyzed transient rheology of discotic mesophases using a tensor order model [14] based on the Landau-de Gennes free energy and found complex stress responses under startup flows of the simple shear. De Andrade Lima and Rey [18] have numerically simulated the Poiseulle flow of DNLCs using the Leslie-Ericksen equations and found multiplicity and multistability of the steady-state solution. The non-Newtonian viscosity of the DNLCs was also analyzed.

In general, both quality and function of products made from the suspension of disklike particles relate to the flow-induced structure of suspensions. Hence the relation between the structural change and the particle motion in suspensions under shear is an interesting subject and such knowledge is useful in the industrial aspect. The Brownian dynamics simulation is an effective technique for that purpose. In the microsimulation that takes account of a particle interaction such as BD and molecular dynamics simulations, the interparticle potential takes an important role to characterize the system considered. In the present study, the Gay-Berne (GB) potential [19] was used as an interparticle potential. This potential has been used as a model potential for the liquid crystalline molecule. Dlugogorski *et al.* [20] and Smondyrev *et al.* [21] have investigated microscopic structures and the rheology of thermotropic liquid crystals by molecular dynamics simulations using the GB potential. Mori *et al.* [22,23] have performed the BD simulation for the system of prolate ellipsoidal particles interacting via the GB potential and investigated the phase transition and the orientational behavior of the system. The simulation indicated that the system of the prolate ellipsoidal particles showed director motions depending on the shear rate such as a continuous rotation, a wagginglike oscillation, and a flow aligning. These studies found that ellipsoidal particles interacting via the GB potential can be employed as a model particle of LCs. In the present study, we investigate the availability of oblate spheroid particles interacting via the GB potential as a model of disklike particles through the BD simulation of the suspension of model particles in a simple shear flow.

II. PARTICLE MODEL AND SIMULATION METHOD

We investigated both the phase transition in an equilibrium state and the orientation behavior of suspension of oblate spheroid particles under simple shear flows. We used the system of suspension of the particles interacting via the Gay-Berne potential [19], given by

$$\phi_{ij}^{GB} = 4\varepsilon(\hat{\mathbf{u}}_i,\hat{\mathbf{u}}_j,\hat{\mathbf{r}}_{ij})\left\{\left(\frac{\sigma_0}{R}\right)^{12} - \left(\frac{\sigma_0}{R}\right)^{6}\right\}, \tag{1}$$

$$R = r_{ij} - \sigma(\hat{\mathbf{u}}_i,\hat{\mathbf{u}}_j,\hat{\mathbf{r}}_{ij}) + \sigma_0, \tag{2}$$

where $\hat{\mathbf{u}}_i$ is a unit vector indicating the orientation of the axis of rotation of a spheroid particle i, $\hat{\mathbf{r}}_{ij}$ is a unit vector, indicating the direction from the centroid of a particle j to that of

a particle i, and r_{ij} is the interparticle distance. The detail of the well depth of the potential $\varepsilon(\hat{\mathbf{u}}_i, \hat{\mathbf{u}}_j, \hat{\mathbf{r}}_{ij})$ and the interparticle separation $\sigma(\hat{\mathbf{u}}_i, \hat{\mathbf{u}}_j, \hat{\mathbf{r}}_{ij})$ are available in the literature [19,22–25]. Here, σ_0 is the characteristic length of particle, which is equal to the major axis of oblate spheroid particles. We employed the same notation used in previous studies [22,23] for parameters of the GB potential: ε_0, ε_r, μ, and ν.

In the present simulation, we fixed the value of ε_r to 5 and considered systems of particles with r_a=0.2 and 0.3, where r_a is the aspect ratio of a spheroid particle. In addition, we applied $(\mu, \nu)=(1, 0.625)$ to the system with r_a=0.2, and $(\mu, \nu)=(1, 1)$ to that with r_a=0.3.

Figure 1 shows the distance dependence of the GB potential for various configurations, where $r_{ij}^* = r_{ij}/\sigma_0$ is the dimensionless separation between the particle centers. Variables with the dimension of length are scaled by σ_0 in the present study. The system is most stable at the end-to-end configuration, as shown in Fig. 1. Since the values of μ and ν are chosen so that the well depths of the potential for the two systems are almost the same, we can investigate the effect of the aspect ratio of a particle independently of the potential strength.

The simulation was performed by solving translational and rotational equations of motion with respect to the centroid of the particles:

$$\mathbf{F}_i^{GB} - \mathbf{F}_i^V + \mathbf{F}_i^B = \mathbf{0}, \tag{3}$$

$$\mathbf{T}_i^{GB} - \mathbf{T}_i^V + \mathbf{T}_i^B = \mathbf{0}, \tag{4}$$

where $\mathbf{F}^{GB}$, $\mathbf{F}^V$, and $\mathbf{F}^B$ are forces that originate from particle interactions via the GB potential, the viscous drag, and Brownian motions, respectively, and the subscript i is a particle index. The notation $\mathbf{T}$ in Eq. (4) means torque and the subscripts are used in the same way as Eq. (3). The present simulation does not include hydrodynamic interactions between the particles.

The force and torque originating from particle interaction via the GB potential, $\mathbf{F}_{ij}^{GB}$ and $\mathbf{T}_{ij}^{GB}$, are given by [24]

$$\mathbf{F}_{ij}^{GB} = -\frac{\partial \phi_{ij}^{GB}}{\partial \hat{\mathbf{r}}_i}, \tag{5}$$

$$\mathbf{T}_{ij}^{GB} = -\hat{\mathbf{u}}_i \times \frac{\partial \phi_{ij}^{GB}}{\partial \hat{\mathbf{u}}_i}. \tag{6}$$

Here, $\mathbf{F}_{ij}^{GB}$ and $\mathbf{T}_{ij}^{GB}$ are, respectively, the interparticle force and torque from a particle i to a particle j. Consequently, $\mathbf{F}_i^{GB}$ and $\mathbf{T}_i^{GB}$ are calculated by $\mathbf{F}_i^{GB}=\Sigma_{j\neq i}^N \mathbf{F}_{ij}^{GB}$ and $\mathbf{T}_i^{GB}=\Sigma_{j\neq i}^N \mathbf{T}_{ij}^{GB}$, where N is the number of particles.

The shear force $\mathbf{F}^V$ and torque $\mathbf{T}^V$ for spheroids are represented by

$$\mathbf{F}_i^V = 3\pi\sigma_0\{X^A \hat{\mathbf{u}}_i\hat{\mathbf{u}}_i + Y^A(\mathbf{I} - \hat{\mathbf{u}}_i\hat{\mathbf{u}}_i)\} \cdot (\mathbf{v}_i - \mathbf{U}), \tag{7}$$

$$\mathbf{T}_i^V = \pi\eta_s\sigma_0^3\{X^C \hat{\mathbf{u}}_i\hat{\mathbf{u}}_i + Y^C(\mathbf{I} - \hat{\mathbf{u}}_i\hat{\mathbf{u}}_i)\} \cdot (\boldsymbol{\omega}_i - \boldsymbol{\Omega}) + Y^H(\boldsymbol{\varepsilon} \cdot \hat{\mathbf{u}}_i\hat{\mathbf{u}}_i):\mathbf{D}, \tag{8}$$

where η_s is the solvent viscosity, $\mathbf{v}_i$ the translational velocity of the particle i, $\mathbf{U}$ the velocity of background fluid, $\boldsymbol{\omega}_i$ the angular velocity of particle i, $\boldsymbol{\Omega}$ the angular velocity of the background fluid, $\boldsymbol{\varepsilon}$ the Eddington's epsilon, and $\mathbf{D}$ the rate of deformation tensor. The resistance functions for the oblate spheroid [26] denoted by X^A, Y^A, X^C, Y^C, and Y^H are used for the calculation of $\mathbf{F}^V$ and $\mathbf{T}^V$. These resistance functions depend on the geometry of particle and are functions of oblateness $s=\sqrt{1-r_a^2}$. The detail of the functions is available in Ref. [26].

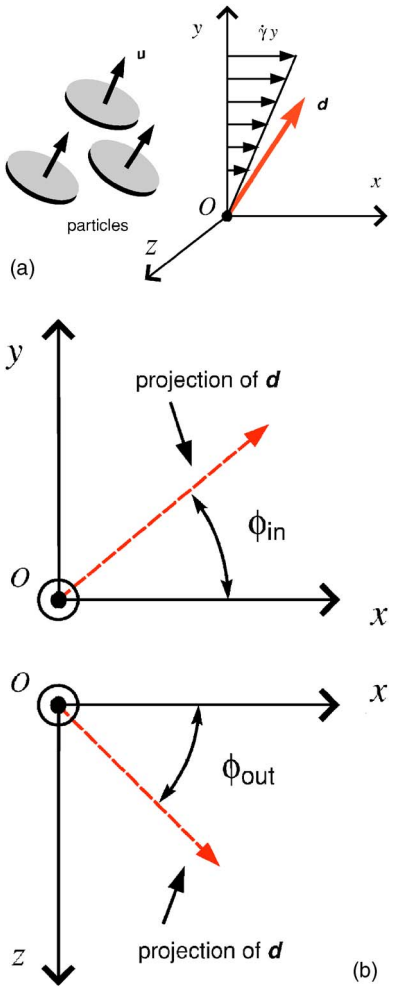

FIG. 2. (Color online) Definition of orientational angles ϕ_{in} and ϕ_{out} and the coordinate system.

Furthermore, the Brownian forces with respect to the directions of primary axes are assumed to be Gaussian:

$$\langle \mathbf{F}^{B\parallel}(\Delta t)\rangle = 0, \quad \langle \mathbf{F}^{B\parallel}(\Delta t) \cdot \mathbf{F}^{B\parallel}(\Delta t)\rangle = \frac{2\zeta_t^{\parallel} k_B T}{\Delta t}, \tag{9}$$

$$\langle \mathbf{F}^{B\perp}(\Delta t)\rangle = 0, \quad \langle \mathbf{F}^{B\perp}(\Delta t) \cdot \mathbf{F}^{B\perp}(\Delta t)\rangle = \frac{2\zeta_t^{\perp} k_B T}{\Delta t}, \tag{10}$$

where the angle bracket denotes the ensemble mean, k_B is the Boltzmann constant, T is the temperature, and $\zeta_t^{\parallel}$ and $\zeta_t^{\perp}$ are the translational friction constants defined by

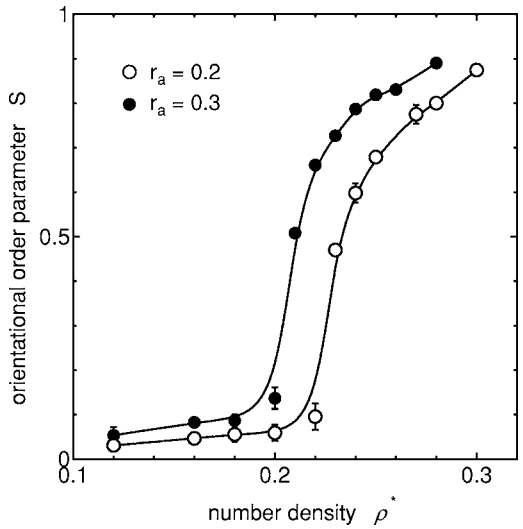

FIG. 3. Orientational order parameter S as a function of the dimensionless number density ρ^* for the systems with r_a=0.2 and 0.3.

$$\zeta_t^{\parallel} = 3\pi\eta_s r_a \sigma_0 X^A, \quad \zeta_t^{\perp} = 3\pi\eta_s r_a \sigma_0 Y^A. \tag{11}$$

The superscripts $\parallel$ and $\perp$ denote the directions parallel and perpendicular to the major axis of the spheroid particle, respectively. Similar relations are assumed for the Brownian torques with respect to the primary axis, $\mathbf{T}^{B\parallel}$ and $\mathbf{T}^{B\perp}$.

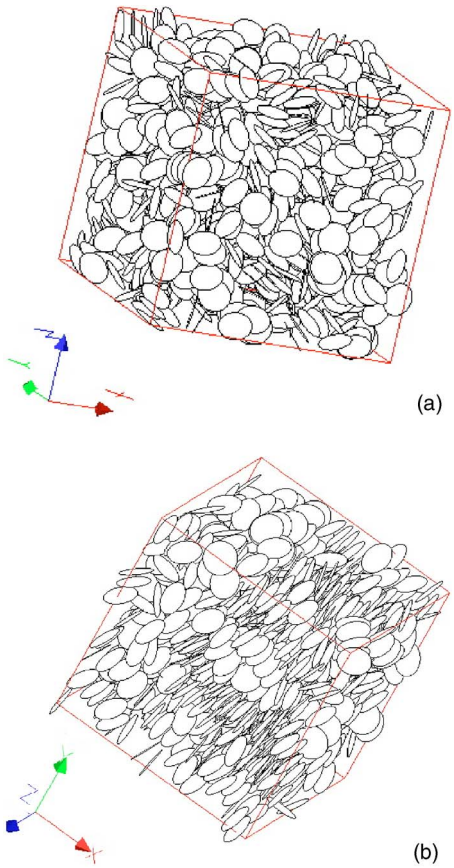

FIG. 4. (Color online) Snapshots of the systems with r_a=0.2 at ρ^*=0.18 (upper) and 0.27 (lower).

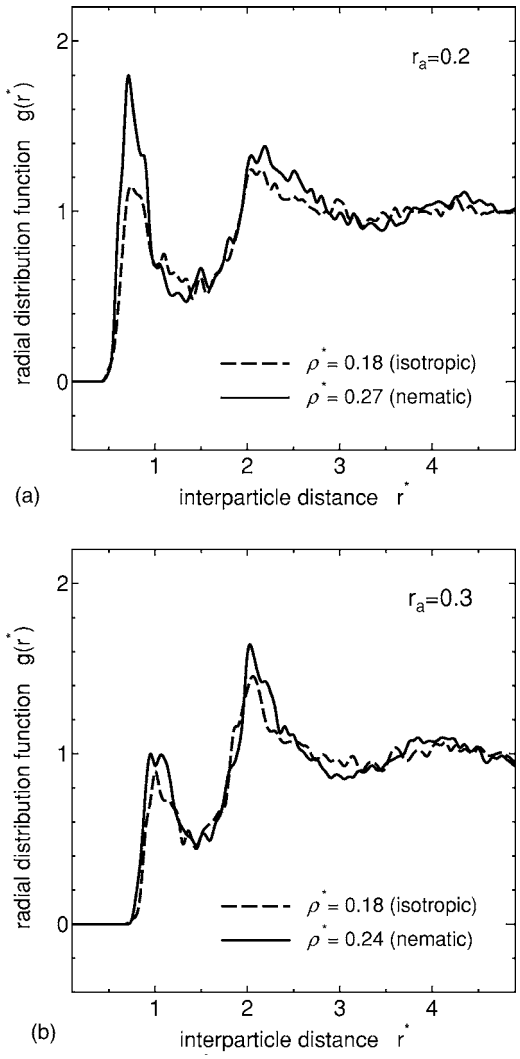

FIG. 5. Radial distribution functions for the systems with r_a =0.2 (a) and 0.3 (b) in isotropic and nematic phases.

The simulations were performed using periodic boundary conditions: The ordinary periodic boundary condition was applied for the simulation at equilibrium state and the Lees-Edwards periodic boundary condition [27] was adopted for the simulation for simple shear flows. The results of simulation at equilibrium are used as initial conditions for the computation of simple shear flow. The simple shear is homogeneously imposed upon the system in a nematic phase at equilibrium. The number of particles N is 864 in a primitive cubic cell for every simulation. The dimensionless temperature was fixed to $T^*=Tk_B/\varepsilon_0=1$. The dimensionless time t^* is defined by t/τ_r, where $\tau_r=3\pi\eta_s\sigma_0/(4k_BT)$.

The orientational behavior of spheroid particles is analyzed using an order parameter and the motion of directors. The order parameter S, defined by

$$S = \sum_i \frac{3\cos^2\beta_i - 1}{2N}, \tag{12}$$

takes a value between 0 and 1: S=0 means the system is in a random state and S=1 indicates a perfect alignment, respec-

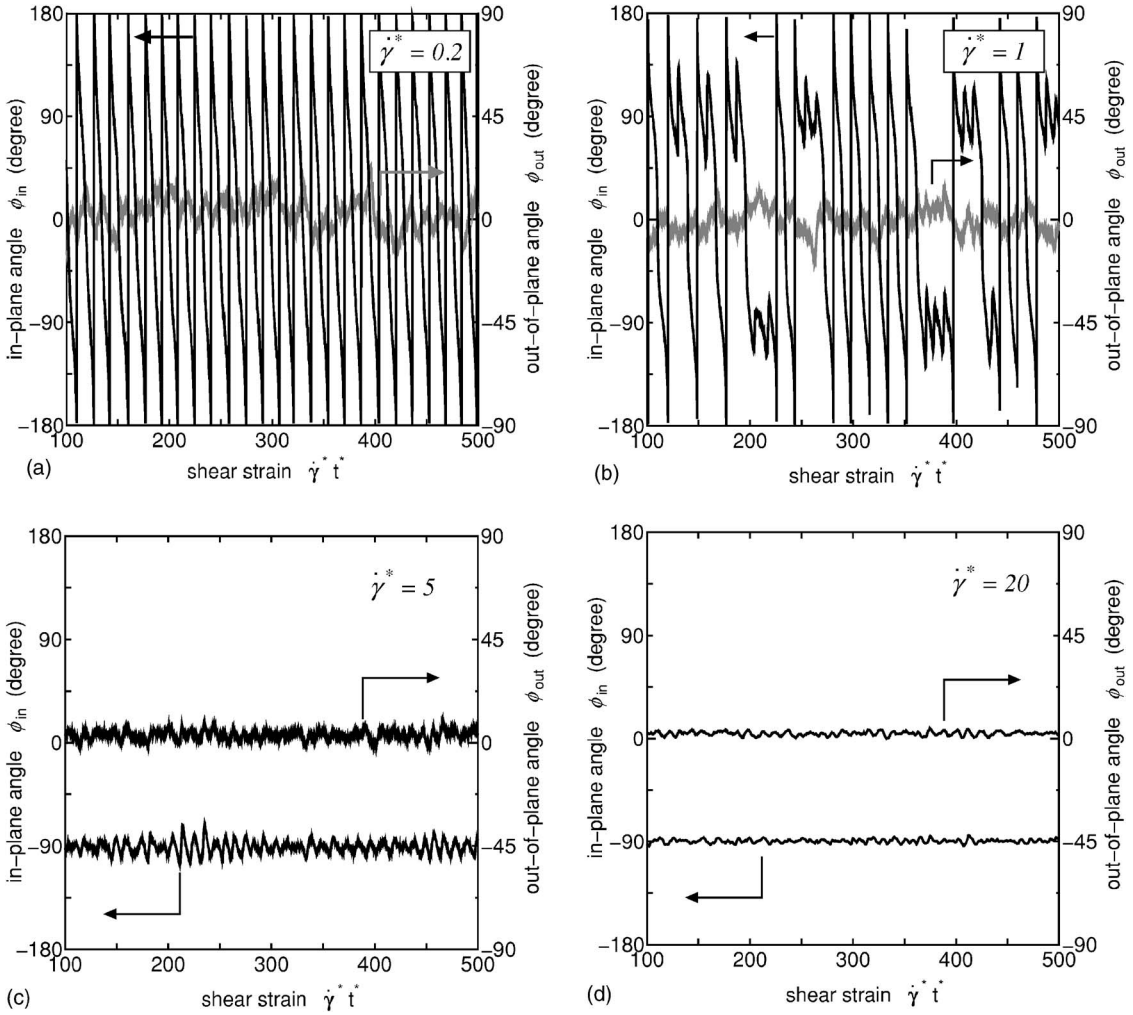

FIG. 6. Temporal change in the orientation angles ϕ_{in} and ϕ_{out} for the system A (r_a=0.2) at $\dot{\gamma}^*$=0.2, 1, 5, and 20.

tively. Here β_i is an angle between a vector, indicating the orientation of the particle i and the director, which is a unit vector indicating the mean orientation of the particles. The director is represented by an in-plane angle ϕ_{in} and an out-of-plane angle ϕ_{out}, as depicted in Fig. 2. The flow direction is parallel to the x axis and the velocity gradient direction is parallel to the y axis, and hence the shear and the vorticity planes are the z-x and the x-y planes, respectively (Fig. 2). The in-plane angle ϕ_{in} is the angle between the projection of the director onto the vorticity plane and the x axis, and ϕ_{out} is the angle between the projection onto the shear plane and the x axis. In addition, we investigated the structure of system using the radial distribution function $g(r^*)$. The radial distribution function is the orientationally averaged pair distribution function, which gives the probability that one particle is separated by a distance of r^* from another particle at the origin and tends to unity in the absence of correlations.

Rheological properties were also predicted using the results of the simulation of simple shear flows. The stress tensor $\boldsymbol{\sigma}$ consists of a term originating from the GB potential $\boldsymbol{\sigma}^p$, the viscous stress $\boldsymbol{\sigma}^v$, an elastic term from Brownian motion $\boldsymbol{\sigma}^e$, and a viscous contribution from Newtonian solvent $\boldsymbol{\sigma}^s = 2\eta_s \mathbf{D}$ [28]:

$$\boldsymbol{\sigma} = \boldsymbol{\sigma}^p + \boldsymbol{\sigma}^v + \boldsymbol{\sigma}^e + \boldsymbol{\sigma}^s. \tag{13}$$

The stress due to the GB potential is described as

$$\boldsymbol{\sigma}^p = \frac{1}{V}\sum_{i=1}^{N-1}\sum_{j>i}^{N} \hat{\mathbf{r}}_{ij}\mathbf{F}_{ij}^{GB}, \tag{14}$$

where V is the volume including N particles. The viscous term has been given by Hinch and Leal [29] as

$$\boldsymbol{\sigma}^v = 2\eta_s\varphi\{A\langle\hat{\mathbf{u}}_i\hat{\mathbf{u}}_i\hat{\mathbf{u}}_i\hat{\mathbf{u}}_i\rangle:\mathbf{D} + B[\langle\hat{\mathbf{u}}_i\hat{\mathbf{u}}_i\rangle:\mathbf{D} + \mathbf{D}:\langle\hat{\mathbf{u}}_i\hat{\mathbf{u}}_i\rangle] + C\mathbf{D} + FDr_0\mathbf{D}\}, \tag{15}$$

where φ is the volume fraction and Dr_0 the rotary diffusivity. For oblate spheroids, the coefficients A, B, C, and F are given by [30]

$$A = -\frac{5}{3\pi r_a} + \left(\frac{104}{9\pi^2} - 1\right), \quad B = -\frac{4}{3\pi r_a} + \left(\frac{1}{2} - \frac{64}{9\pi^2}\right),$$

$$C = \frac{8}{3\pi r_a} + O(r_a), \quad F = -\frac{12}{\pi r_a} + O(r_a). \tag{16}$$

The elastic term for spheroid particles is expressed by [28]

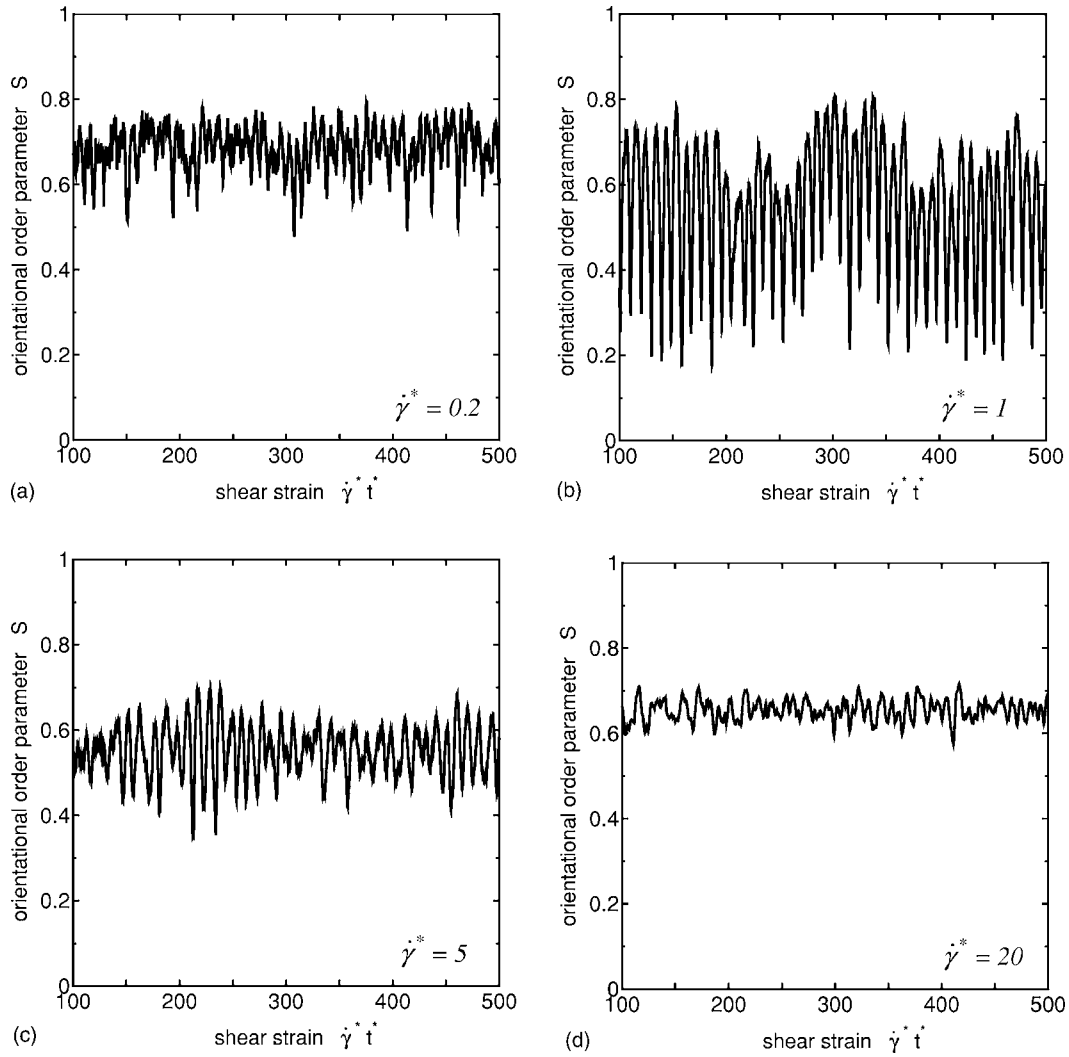

FIG. 7. Temporal change in the order parameters S for the system A (r_a=0.2) at $\dot{\gamma}^*$=0.2, 1, 5, and 20.

$$\boldsymbol{\sigma}^e = \sum_{i=1}^{N} 3\left(\frac{r_a^2-1}{r_a^2+1}\right)\nu k_B T\langle \hat{\mathbf{u}}_i\hat{\mathbf{u}}_i\rangle. \tag{17}$$

The stress tensors σ^p, σ^v, σ^e, and σ^s are scaled by $4\varepsilon_0/\sigma_0^3$ in the present study. The shear stress $\boldsymbol{\sigma}_{yx}$ and the normal stress difference are investigated. The first and the second normal stress differences N_1 and N_2 are defined by

$$N_1 = \sigma_{xx} - \sigma_{yy}, \tag{18}$$

$$N_2 = \sigma_{yy} - \sigma_{zz}. \tag{19}$$

III. RESULTS AND DISCUSSION

A. Phase transition at equilibrium

We first analyzed the phase transition due to density change. Figure 3 shows the dependence of the orientational order parameter S on the dimensionless number density of the particles $\rho^*(=\rho\sigma_0^3)$. In both cases, the value of S increases and the system changes from an isotropic phase to a nematic one with increasing ρ^*. The system with more planular particles translates to a nematic phase at a higher number density, i.e., r_a=0.2. Since the value of the interparticle distance at the peak of potential is small for r_a=0.2, as compared to the that for r_a=0.3, as shown in Fig. 1, a higher number density is required for the phase transition to a nematic state. If the comparison at the same volume ratio was carried out, one can find that the phase transition occurs at a lower volume ratio for the system with more planular particles.

Snapshots of the system with r_a=0.2 at ρ^*=0.18 and 0.27 are depicted in Fig. 4. In the system with ρ^*=0.18, the particles randomly orientate and the system is in an isotropic phase, while the system with ρ^*=0.27 has a certain degree of order in the particle orientation and is in a nematic phase. In addition, a columnar structure is partially seen in the nematic phase at ρ^*=0.27. This fact is confirmed in the results of radial distribution functions $g(r^*)$ in nematic phases shown in Fig. 5(a). The distribution has two peaks at $r^* \simeq 0.8$ and 2: the first peak at r^* of about 0.8 corresponds to the end-to-end configuration of particles and the second peak corresponds to the side-by-side configuration, which means a columnar structure is formed in the system. These results imply that a

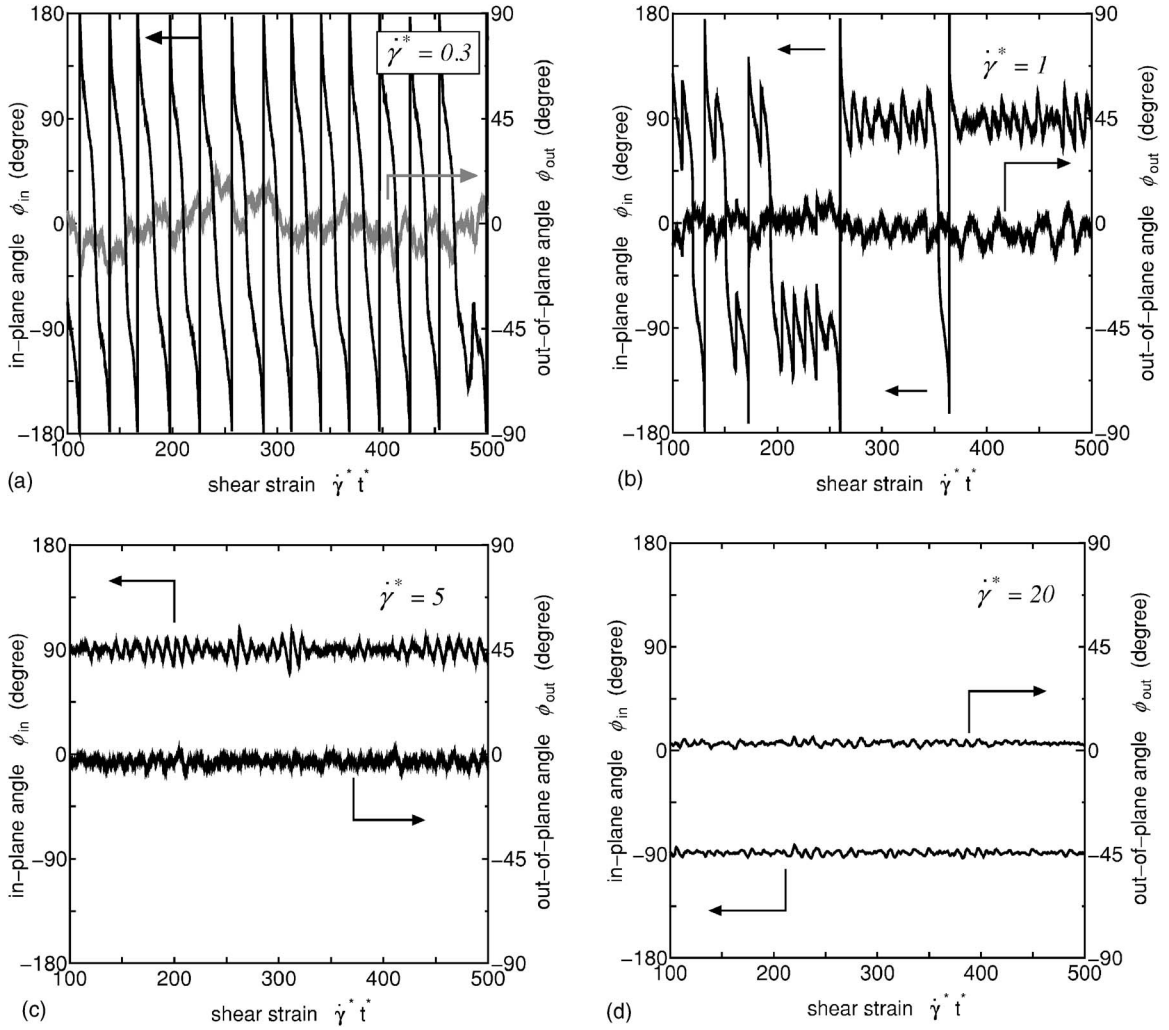

FIG. 8. Temporal change in the orientation angles ϕ_{in} and ϕ_{out} for the system B (r_a=0.3) at $\dot{\gamma}^*$=0.3, 1, 5, and 20.

columnar structure is easily configurated oblate spheroidal particles interacting via the GB potential. In addition, it should be noted here that although the columnar structure is partially seen, the global configuration of the particle centroid is random and hence the system is considered to be in a nematic phase. In Fig. 5, two peaks are observed in each system and $g(r^*)$ at each peak is larger in the nematic phase than that in the isotropic phase. The first peak for the system with r_a=0.3 is not outstanding as compared to the corresponding results for r_a=0.2. This fact means that a remarkable columnar structure is not observed in the system with r_a=0.3. For an orientationally ordered system, correlation functions parallel and perpendicular to the director are often applied to the analysis of microstructures [25]. The longitudinal distribution function $g_{\parallel}(r_{\parallel}^*)$ gives the probability of finding a particle at a distance $r_{\parallel}^*$, which is the pair separation parallel to the director. On the other hand, the in-plane distribution function $g_{\perp}(r_{\perp}^*)$ gives information on the positional correlations within a layer, where $r_{\perp}^*$ is the pair separation perpendicular to the director. We confirmed that the distribution of $g_{\parallel}(r_{\parallel}^*)$ showed a featureless uniform distribution, which means the system is in the nematic phase; for the smectic phase, a periodic order along the director is observed [25]. This result indicates that the columnar structure does not have long-range ordering but has short-range ordering, which coincides with the observation of snapshots. In addition, the distribution of $g_{\perp}(r_{\perp}^*)$ shows two peaks that correspond to the end-to-end and the side-by-side configurations similar to that observed in $g(r^*)$, and additional information on microstructures is not obtained. Thus, we analyzed the structural change in shear flows base on the basis of $g(r^*)$ in the following discussion.

B. Simple shear flow

We next analyze the orientational behavior of particles under simple shear flows at various shear rates $\dot{\gamma}$. The shear is imposed upon a system at equilibrium at t^*=0. We chose two systems with (ρ^*, r_a, S_{eq})=(0.27, 0.2, 0.78) and (0.24, 0.3, 0.79), which are nematic at equilibrium. Here, S_{eq} is the orientational order parameter at equilibrium. The former and latter systems are, respectively, denoted as systems A and B. The volume fraction φ is 0.28 for the former system and is 0.37 for the latter. In addition, we considered also a system with r_a=0.3 of ρ^*=0.18 and φ=0.28, system C, to compare rheological properties of the system with r_a=0.2 and those

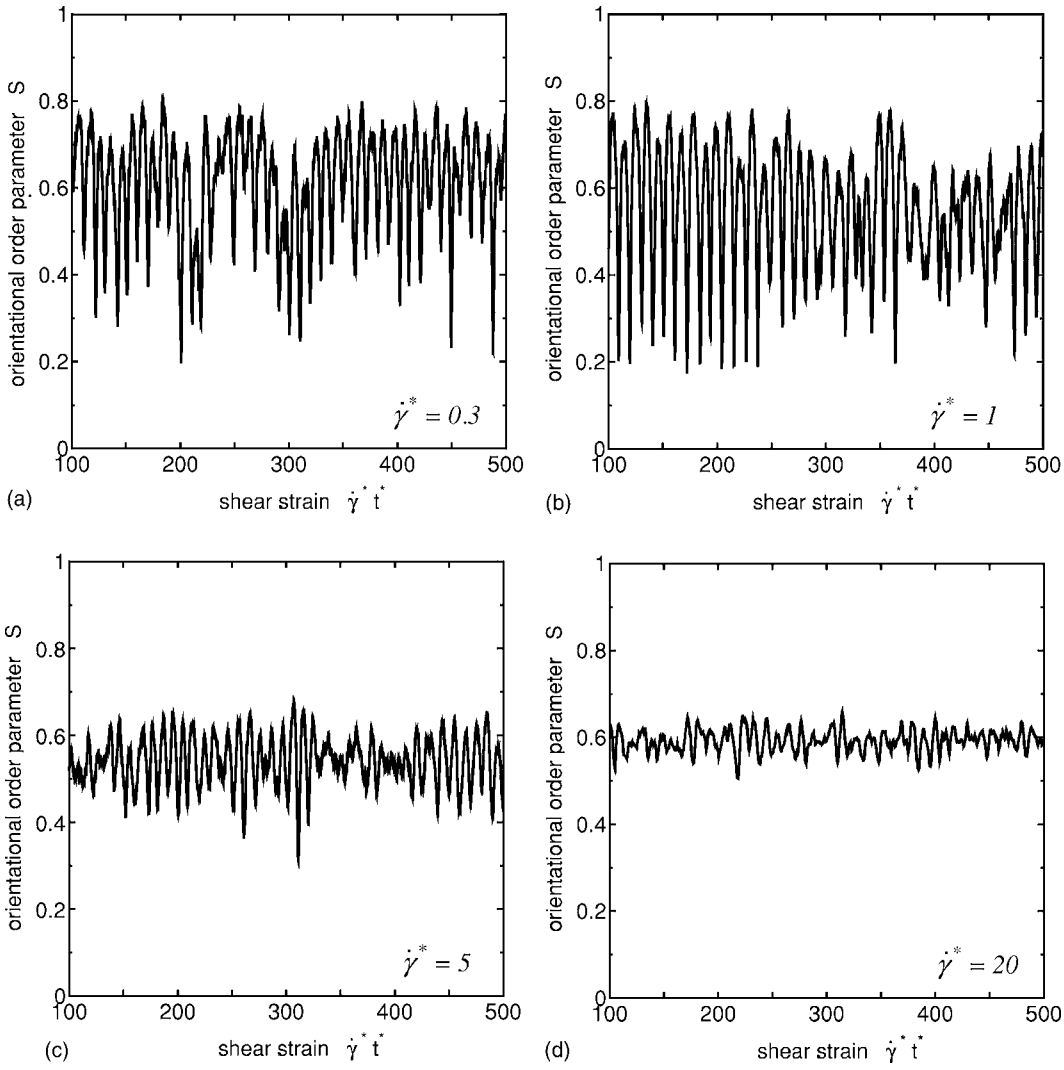

FIG. 9. Temporal change in the order parameters S for the system B (r_a=0.3) at $\dot{\gamma}^*$=0.3, 1, 5, and 20.

with r_a=0.3 at the same volume ratio; the system C is isotropic at equilibrium.

Figures 6 and 7, respectively, show temporal changes in the orientational angles, ϕ_{in} and ϕ_{out}, and the orientational order parameter S of the system A after the imposition of the shear flow at dimensionless shear rates $\dot{\gamma}^*(=\dot{\gamma}\tau_r)$ of 0.2, 1, 5, and 20. The director continuously rotates slightly out of the shear plane at low shear rates. At high shear rates, the flow aligning is predicted: The orientation angles keep almost constant values and S is relatively large.

As shown in Figs. 6(a) and 6(b), the period of change in ϕ_{in} at $\dot{\gamma}^*$=0.2 is similar to that at $\dot{\gamma}^*$=1 when the director continuously rotates and hence the period shows little dependence on the shear rate. At $\dot{\gamma}^*$=1, we can see a director motion that the director hesitates to rotate, which is called wagging. The wagging motion of director was predicted also in a study of microstructural response of discotic nematic liquid crystals in a simple shear flow using constitutive equations [11,13]. The wagging occurs also at $\dot{\gamma}^*$=5, even though it is not seen outstandingly because the amplitude is small. The wagging motions at these shear rates are confirmed later by the frequency analysis of a wave shape of ϕ_{in}. In Figs. 7(b) and 7(c), the order parameter S fluctuates largely and the average of S is relatively small during the director is wagging at $\dot{\gamma}^*$=1 and 5. The wagging is a cause of the decrease in S and the large fluctuation. At higher shear rate, $\dot{\gamma}^*$=20, the system is in a flow-aligning state. Both ϕ_{in} and ϕ_{out} keep almost constant angles, as shown in Figs. 6(d). In addition, S is relatively large and the fluctuation in S is small. At high shear rates, the director orientates to the velocity gradient direction, i.e., particles are mostly aligned to the flow direction, and this prediction agrees with the experimental results for suspensions of disklike particles [6–8]. The shear-rate dependence of the director motion is explained as follows: When the shear rate is low, the particle interaction is relatively strong and the particles rotate in phase, and hence the director rotates. As the shear rate increases, the effect of shear flow intensifies and the effect of particle interaction becomes relatively weak. Hence, at high shear rates the particles are hard to rotate in phase and rotate independently. As a result, the director does not rotate and the flow aligning occurs.

In the case of the system B, qualitatively the same results are obtained, as shown in Figs. 8 and 9: We can see the continuous rotation and the wagging motion at low to mod-

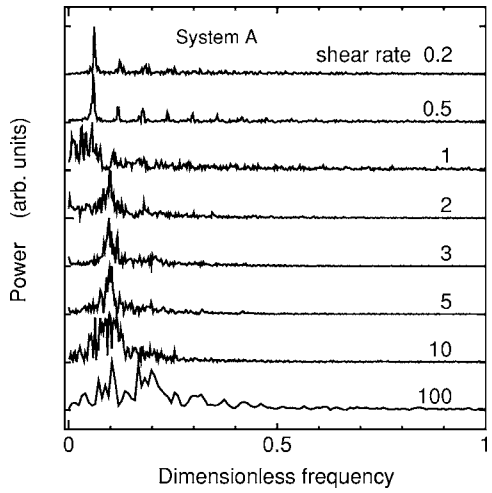

FIG. 10. Power spectrum of the wave form of temporal change in the in-plane-angle ϕ_{in} for the system A (r_a=0.2) at $\dot{\gamma}^*$=0.2, 0.5, 1, 2, 3, 5, 10, and 100: Data at each shear rate are shifted in the vertical direction for an easy comparison.

erate shear rates and the flow aligning at high shear rates.

We next analyze the wave shapes of temporal change in ϕ_{in} using the Fourier transformation to confirm the pattern of the director motion. Figure 10 shows the power spectrum of the wave form of a temporal change in ϕ_{in}. When the director continuously rotates, at low shear rates $\dot{\gamma}^*$=0.2 and 0.5, the power spectra are found to indicate periodic behavior. At $\dot{\gamma}^*$=1, the shape of spectrum collapses because continuous rotation and wagging motion coexist at this shear rate. As the shear rate increases, at $\dot{\gamma}^*$=2, 3, and 5, the peak position shifts to the higher-frequency side and the distribution of the spectrum broadens. These results indicate that the director does not rotate continuously and is wagging in this region. When the shear rate further increases, at shear rates of more than 10, the distribution of the power spectrum is broad and hence no periodic behavior occurs, i.e., the system is in a flow-aligning state.

Figure 11 shows the shear-rate dependence of the time-averaged orientational order parameter S_{av}. The error bars indicate the variance. The marks in the figure denote the type of director motion at corresponding shear rates, i.e., rotation, wagging, and aligning. In the simulation of simple shear flows, we focus on the orientational behavior of the systems A and B, which are in a nematic phase at equilibrium. In Fig. 11, however, we also plot the results for the system C, which is considered later in the analysis of rheological properties. The system C is isotropic and S_{av} is low at equilibrium, and S_{av} increases consistently with the shear rate to approach a value at high shear rates.

For both the systems A and B, S_{av} is relatively high at low shear rates because the systems are in a nematic phase. In the range of low shear rates, S_{av} decreases with increasing the shear rate because of the director rotation. The order parameter takes the minimum at a shear rate where the director is wagging. Larson [31] has numerically computed shear flows of rodlike LCPs using the Doi equation [32]. The numerical simulation predicted director motions such as tumbling at low shear rates, a transition from tumbling to wagging at

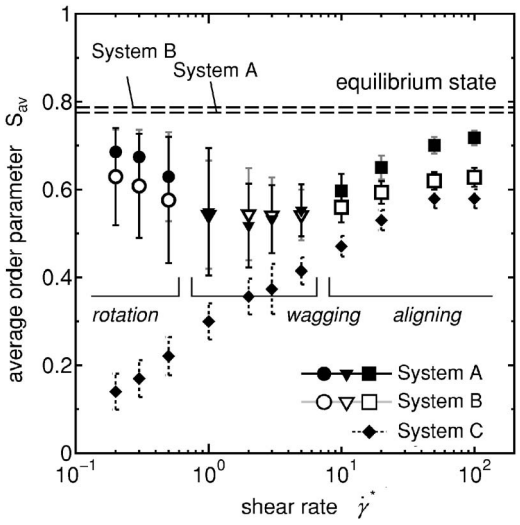

FIG. 11. Average orientational order parameter S_{av} as a function of shear rate $\dot{\gamma}^*$. The marks represent the behavior of suspension: circles, triangles, and squares indicate rotation, wagging, and aligning, respectively.

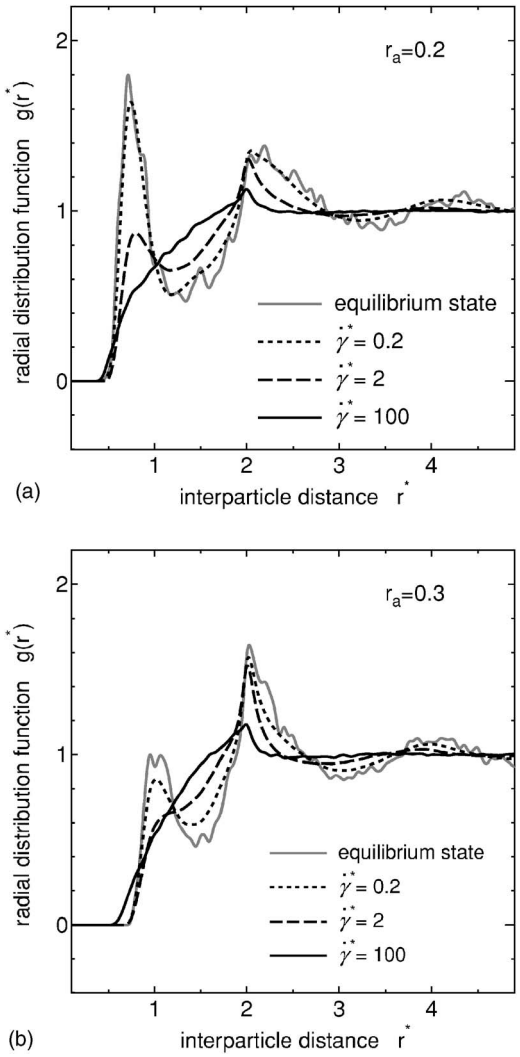

FIG. 12. Average radial distribution function for the systems A (r_a=0.2, a) and B (r_a=0.3, b) at $\dot{\gamma}^*$=0.2, 2, and 100.

moderate shear rates, and flow aligning at high shear rates. In addition, it is numerically predicted by computing the Doi equation directly without closure approximations that the order parameter of liquid crystalline systems under simple shear flows decreases when the director is wagging [33,34]. The results of the BD simulation coincide with these predictions. At higher shear rates, where the system is in the aligning state, S_{av} increases consistently with $\dot{\gamma}^*$. The order parameter is higher for the system with more disklike particles, i.e. the system A, in the rotation and aligning regions, while in the wagging region, the order parameter takes similar low values for the systems A and B.

Figure 12 shows time-averaged radial distribution functions $g(r^*)$ for the systems A and B at $\dot{\gamma}^*=0.2$, 2, and 100. The radial distribution functions are averaged over a long enough range of shear strain $\dot{\gamma}^* t^*$ around 500 to 800. Although the in-plane distribution function $g_\perp(r_\perp)$ is often applied to the structural analysis for orientationally ordered systems, we will indicate and analyze the structural change in $g(r^*)$ alone because the distribution of $g_\perp(r_\perp)$ also shows a similar behavior to $g(r^*)$ in the present simulation. The initial structure of each system at equilibrium collapses and short columnar structures diminish as the shear rate increases. For both systems, the first peak at r^* of about 0.8 disappears at $\dot{\gamma}^*=100$. This result means that the interparticle distance widens at high shear rates. As a result, particles easily rotate independently and do not rotate in phase; hence, the temporal change in the director motion is very small and ϕ_{in} and ϕ_{out} are almost constant.

Finally, we analyze rheological properties of the system of oblate spheroid particles. The shear stress and viscosity are generally affected by the geometrical relation between the orientation of the director and the flow direction. Hence, the Miesowicz viscosities are often considered to investigate shear properties of anisotropic liquids: The viscosities are measured when the director is locked and the shear is imposed on a liquid under three geometrical conditions that the director is parallel to the flow, parallel to the velocity gradient, and perpendicular to both the flow and the velocity gradient. On the other hand, in the present simulation we consider the stresses when the director is not locked and rotates freely because it is a similar condition to flows in a rheometer and, furthermore, the order parameter S of the present system is affected by the lock of director using an external force unlike low molecular liquid crystals, and the stress field changes.

In the present simulation, rheological properties such as shear and normal stresses do not depend on the geometrical relation between the initial orientation of director at equilibrium and the flow direction if enough large strain is imposed on a system. Thus, we considered time-averaged stresses over a long period after the transient region just after the onset of shear flow to investigate rheological properties of the system. At high shear rates, the system is flow aligning and hence the stresses are similar to the Miesowicz stresses when the director is parallel to the velocity gradient.

Figure 13 shows the dimensionless shear stress σ^*_{yx} and the dimensionless first and second normal stress differences, N^*_1 and N^*_2, for the systems A, B, and C. The stresses are

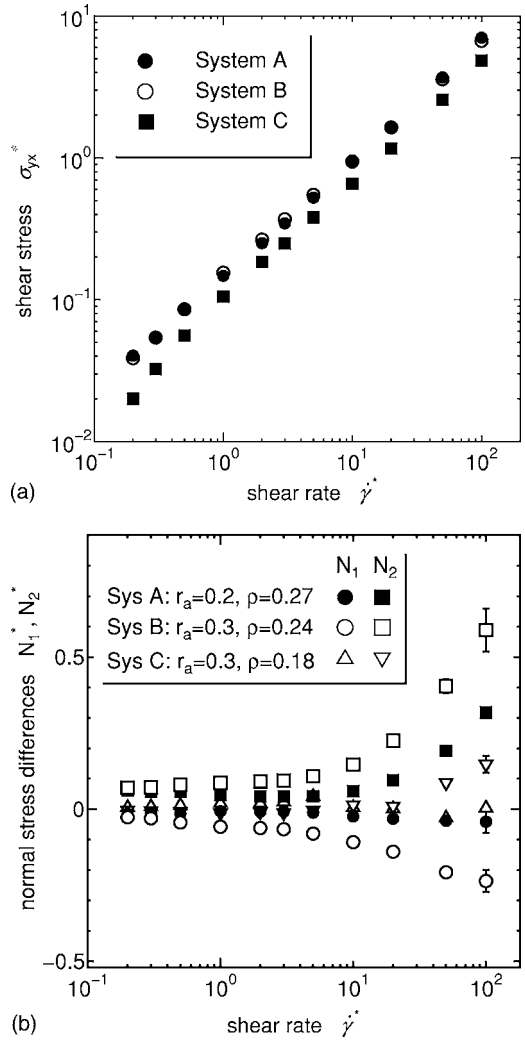

FIG. 13. Rheological properties of the systems A, B, and C: (a) shear stress σ^*_{yx}; (b) first and second normal stress differences, N^*_1 and N^*_2.

evaluated using average values over a long enough range of shear strain $\dot{\gamma}^* t^*$ around 500 to 800. The error bars indicate the variance. The gradient of the flow curve, σ^*_{yx} vs $\dot{\gamma}^*$, correspond to the apparent shear viscosity defined by the ratio of shear stress to shear rate. As shown in Fig. 13(a), the slope of flow curve decreases with increasing the shear rate, which means the viscosity has a shear-thinning property. At very high shear rates the flow curves tend to be linear, and this result implies that the viscosity has a plateau region. The prediction of the shear-thinning property and the existence of the plateau region in apparent shear viscosity agrees with the predictions using a constitutive equation for discotic nematics proposed by Singh and Rey [11,12] and with experimental results [35,36]. Moreover, negative N^*_1 and positive N^*_2 are predicted, and the magnitude of the normal stress differences rapidly increases at high shear rates. These predictions also qualitatively agree with the predictions by Singh and Rey [11,12]. Thus, the system with oblate spheroid particles has the capability of simulating the rheological properties of suspensions of disklike particles.

In Fig. 13(a), the viscosities of the systems A and B are similar and higher than that of the system C. At high shear rates, the systems are flow aligning and the orientational order is relatively high, and hence the resistance to the flow decreases. Consequently, the apparent viscosity decreases with increasing the shear rate. The shear-thinning property in viscosity is seen for the three systems and the shear-thinning effect appears more strongly for the system of more disklike particles when the volume ratio is similar.

In the results of the normal stress difference in Fig. 13(b) for the system C that is isotropic at equilibrium, the normal forces do not appear in a wide range of shear rates and N_2^* appears only at very high shear rates. On the other hand, for the system A that consists of particles with $r_a=0.2$ and the volume ratio is similar to that of the system C, both N_1^* and N_2^* appear at moderate shear rates and their magnitudes are larger than the counterparts of the system C. Consequently, larger normal stress difference emerges for the system of more disklike particles. Large normal stress differences are predicted for the system B as compared to the results for the systems A and C. This is because the volume ratio of the system is highest in the three systems.

IV. CONCLUSION

The Brownian dynamics simulation has been carried out for suspensions of oblate spheroid particles interacting via the Gay-Berne potential. The BD simulation predicted the phase transition due to the particle concentration. The system with more disklike particles translates to the nematic phase at a higher number density. Furthermore, the simulation under simple shear flows predicted the dependence of director motion on the shear rate and found that the director continuously rotated at low shear rates, showed the wagging motion at moderate shear rates, and was aligned at high shear rates. As the shear rate increases, the average order parameter S_{av} decreases in the rotational state and increases in the flow-aligning state. The order parameter took the minimum in the wagging state. The inner structure of suspension was also analyzed to find that a short columnar structure at equilibrium in nematic phase collapses during the shear flow. Moreover, the predictions of rheological properties such as the shear stress and the normal stress difference qualitatively agreed with the counterparts predicted using a constitutive equation [11,12]. The shear viscosity of suspensions of oblate spheroid particles shows shear-thinning property. The magnitude of normal stress difference is larger for the system with more disklike particles. The present study proves that the BD simulation using spheroid particles interacting via the GB potential is an effective approach for investigating the flow behavior and flow-induced structure of suspensions of disklike particles at a particulate level.

[1] S. M. Jogun and C. F. Zukoski, J. Rheol. **40**, 1211 (1996).
[2] S. M. Jogun and C. F. Zukoski, J. Rheol. **43**, 847 (1999).
[3] A. B. D. Brown, S. M. Clarke, P. Convert, and A. D. Rennie, J. Rheol. **44**, 221 (2000).
[4] M. Moan, T. Aubry, and F. Bossard, J. Rheol. **47**, 1493 (2003).
[5] B. Hammouda, J. Mang, and S. Kumar, Phys. Rev. E **51**, 6282 (1995).
[6] A. B. D. Brown, S. M. Clarke, and A. R. Rennie, Langmuir **14**, 3129 (1998).
[7] A. B. D. Brown and A. R. Rennie, Phys. Rev. E **62**, 851 (2000).
[8] A. B. D. Brown and A. R. Rennie, Chem. Eng. Sci. **56**, 2999 (2001).
[9] T. Carlsson, Mol. Cryst. Liq. Cryst. **89**, 57 (1982).
[10] T. Carlsson, Mol. Cryst. Liq. Cryst. **104**, 307 (1984).
[11] A. P. Singh and A. D. Rey, Rheol. Acta **37**, 30 (1998).
[12] A. P. Singh and A. D. Rey, Rheol. Acta **37**, 374 (1998).
[13] A. P. Singh and A. D. Rey, J. Non-Newtonian Fluid Mech. **94**, 87 (2000).
[14] T. Tsuji and A. D. Rey, J. Non-Newtonian Fluid Mech. **73**, 127 (1997).
[15] A. D. Rey and T. Tsuji, Macromol. Theory Simul. **7**, 623 (1998).
[16] T. Tsuji and A. D. Rey, Phys. Rev. E **57**, 5609 (1998).
[17] D. Grecov and A. D. Rey, Rheol. Acta **42**, 590 (2003).
[18] L. P. R. de Andrade Lima and A. D. Rey, J. Non-Newtonian Fluid Mech. **110**, 103 (2003).
[19] J. G. Gay and B. J. Berne, J. Chem. Phys. **74**, 3316 (1981).
[20] B. Z. Dlugogorski, M. Grmela, and P. J. Carreau, J. Non-Newtonian Fluid Mech. **53**, 25 (1994).
[21] A. M. Smondyrev, G. B. Loriot, and R. A. Pelcovits, Phys. Rev. Lett. **75**, 2340 (1995).
[22] N. Mori, R. Semura, and K. Nakamura, Mol. Cryst. Liq. Cryst. Sci. Technol., Sect. A **367**, 445 (2001).
[23] N. Mori, H. Fujioka, R. Semura, and K. Nakamura, Rheol. Acta **42**, 102 (2003).
[24] G. R. Luckhurst and R. A. Stephens, Liq. Cryst. **8**, 451 (1990).
[25] M. A. Bates and G. R. Luckhurst, J. Chem. Phys. **110**, 7087 (1999).
[26] S. Kim and S. J. Karrila, *Micro-hydrodynamics: Principle and Selected Applications* (Butterworth-Heinemann, Stoneham, 1991).
[27] A. W. Lees and S. F. Edwards, J. Phys. C **5**, 1921 (1972).
[28] R. G. Larson, *The Structure and Rheology of Complex Fluids* (Oxford University Press, New York, 1999).
[29] E. J. Hinch and L. G. Leal, J. Fluid Mech. **57**, 753 (1973).
[30] E. J. Hinch and L. G. Leal, J. Fluid Mech. **52**, 683 (1972).
[31] R. G. Larson, Macromolecules **23**, 3983 (1990).
[32] M. Doi, J. Polym. Sci., Polym. Phys. Ed. **19**, 229 (1981).
[33] S. Chono, T. Tsuji, and A. Taniguchi, Trans. Jpn. Soc. Mech. Eng., Ser. B **62**, 600 (1996).
[34] S. Chono and T. Tsuji, Trans. Jpn. Soc. Mech. Eng., Ser. B **65**, 3539 (1999).
[35] B. Fathollahi and J. L. White, J. Rheol. **38**, 1591 (1994).
[36] A. D. Cato and D. D. Edie, Carbon **41**, 1411 (2003).